Journal of the Serbian Society for Computational Mechanics / Vol. 15 / No. 2, 2021 / pp 63-78
(10.24874/jsscm.2021.15.02.07)

PARAMETRIC INVESTIGATION OF BAND GAP EFFECTS IN CHIRAL MICROSTRUCTURES

Panagiotis Koutsianitis, Georgios K. Tairidis, Alexandros Kougkoulos, Georgios E. Stavroulakis*

School of Production Engineering and Management, Computational Mechanics and Optimization Lab, Technical University of Crete, Chania, Crete, Greece
e-mail: panoskout@gmail.com, tairidis@gmail.com, nioabc@gmail.com, gestavr@dpem.tuc.gr
**corresponding author*

Abstract

Vibration suppression has been thoroughly studied in the last few years. A number of methods has been proposed for this purpose. An evolving method lies in the search of band gap regions, that is, certain frequency ranges where vibrations are isolated. In the present investigation, a periodic unit cell of a chiral metamaterial has been created in order to study its dynamic behavior and how this affects the wave propagation into a lattice structure consisting of repeated chiral microstructures. Each cell represents a composite structure consisted by a soft matrix with hard connector wings and a circular core. The system is studied by plane stress finite elements. The design parameters of the structure that define the shape and the material are modified in order to study the changes at the appearance of the band gap areas. In addition, results of the dynamic response of the structure in the frequency domain will be presented in order to show the magnitude of the vibration reduction that can be achieved in a specific frequency range.

Keywords: Chiral metamaterials, band gaps, vibration isolation, Bloch theory

1. Introduction

For the study of wave propagation, the pioneering work of Brillouin (1953) and Kittel (1962) should be considered. According to these references, specific frequencies where the wave is able or unable to propagate through a structure may occur, which are called pass and stop band gaps. The propagation of the wave in two-dimensional periodic structures is described in (Srikantha Phani et al. 2006), (Mace et al. 2008). Periodic structures filled with polymer and the effects of different types of filling are studied in (Hsiang-Wen et al. 2017). It is shown that wide band gap areas appear at the unfilled structure, which can be used in vibration isolation and acoustic filters. It is also shown that the auxeticity affects the propagation of the wave through the periodic structure (Outzen et al. 2019).

Auxeticity is an interesting property of some materials which present negative Poisson's ratio, that is, the structural elements tend to expand, when stretched, while conventional materials tend to narrow. These mechanical metamaterials are called auxetic materials. Among the interesting properties of auxetics is also the enhanced vibration suppression (Ma et al. 2013). Auxetic materials usually have peculiar shapes, such as star-shaped and chiral microstructures,

or even more complicated forms which occur from topology optimization. More information on the auxetic materials can be found in the recent review (Duncan et al. 2018). There are several papers in recent literature which study the effect of the properties of microstructures, and especially of the ones with auxetic behavior, in the isolation of vibrations and the creation of band gap areas in specific frequencies (Meng et al. 2015), (Chen et al. 2018), (Bacigalupo et al. 2015), (Koutsianitis et al. 2019).

Chiral metamaterials present interesting mechanical properties due to the coupling of longitudinal with rotational deformation. Among others, auxetic behaviour and band gap appearance have been observed, see (Wu et al. 2019) and the references given there. This transfer of deformation mode can be exploited in dynamics and leads to interesting band gaps that can be used for technical applications. Classical or topology optimization can be used in order to fine tune the band gap formation and design the microstructure with respect to required properties. The basic mechanism is the transfer of kinetic energy from large to small scale, where it is damped.

Further information related to this topic can be found in recent literature: analytical investigation of the inertial amplification mechanism in (Yilmaz 2018), hexagonal chiral latices in (Spadoni et al. 2009), three-dimensional anti-chiral auxetic metamaterials with tunable phononic bandgaps (Fei et al. 2020), hybrid reentrant and anti-chiral materials in (Qi et al. 2019), hybrid reentrant honeycombs (Xin et al. 2021), optimal design of chiral in (Chen et al. 2021), (Hosseinkhani et al. 2021), (Bacigalupo et al. 2019). It should be also emphasized that the developments in additive manufacturing make the usage of complicated metamaterials feasible (Matlack et al. 2016), (Askari et al. 2020).

In the present investigation, a model which consists of two-dimensional chiral microstructures is studied, using finite element analysis, in order to demonstrate the band gap properties. The parametric investigation presented here can be extended and coupled with optimal design algorithms for more detailed investigation.

The paper is organized as follows: in Section 2, the fundamental relations, that is, the Bloch theory for 2D elements is presented. Section 3 is devoted to the numerical results of the study. Finally, in Section 4 the conclusions of the investigation are given.

2. Bloch theory for 2D elements

An assembly of structural elements (e.g. beams, rectangular elements, square elements, etc.) is called lattice and it is produced from the correlation between the unit cell and the basis vectors ε_i. In this direction, the suitable definition of a unit cell is critical. It is also necessary to define the lattice points r_j of a unit cell, which are a subset of the nodes of the total finite element model. In the present paper, 2D lattices which consist of plane stress elements are considered.

The displacement $q(r_j)$ of the lattice points of the unit cell for plane waves, is defined as:

$$q(r_j) = q_j e^{(i\omega t - k r_j)} \tag{1}$$

where q_j is the amplitude, ω is the frequency, and k is the wave vector, respectively.

There are two parameters n_1 and n_2, which can identify any other unit cell, and can be obtained by n translations across the e directions with respect to each specific unit cell. According to Bloch's theorem the displacement at the j^{th} point of any unit cell can be identified by such a unique pair of integers n_1 and n_2 as:

$$q = q(r_j)e^{k(r-r_j)} = q(r_j)e^{(k_1 n_1 + k_2 n_2)} \tag{2}$$

where:

$$k_1 = ke_1 = \delta_1 + i\varepsilon_1 \tag{3}$$

$$k_2 = ke_2 = \delta_2 + i\varepsilon_2 \tag{4}$$

The complex numbers k_1 and k_2 of Equations 3 and 4 denote the components of the wave vector k which is propagated and dissipated along the vectors e_1 and e_2. The real part δ is the attenuation constant, that is, a measurement of wave propagation among the cells, and the imaginary part ε is the phase constant and it represents the phase change across the unit cell. If there is no attenuation in wave propagation, then the real part δ is zero and the wave vector can be expressed as:

$$k_1 = i\varepsilon_1 \tag{5}$$

$$k_2 = i\varepsilon_2 \tag{6}$$

The first Brillouin zone of a square unit cell with two axis of symmetry P2mm is shown in Fig. 1. The band gaps are created using the assumption that the wave vectors follow the Brillouin zone (Γ-X-M-Y) according to Maurin et al. (2018).

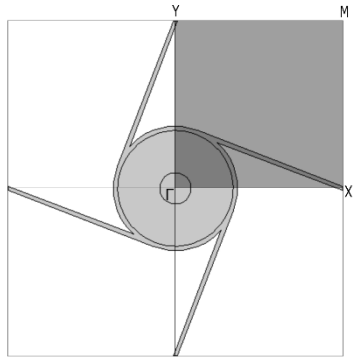

Fig. 1. The first Brillouin zone and the irreducible Brillouin zone (Γ – X – M - Y).

Periodic structures are repetitive geometric patterns. Uniform 2D structures constitute a special case of periodic structures, homogeneous in x and y directions, as an assembly of rectangular segments with length L_x and L_y to the x and y directions, respectively.

The scheme shown in Fig. 2, suggests that the degrees of freedom q of the rectangular segment of reference can be considered with respect to the nodal degrees of freedom as:

$$q = \left[q_1^T \; q_2^T \; q_3^T \; q_4^T \right] \tag{7}$$

where q_j are the nodal degrees of freedom of the nodes of the jth corner of the segment, while the superscript T denotes the transpose.

The equations of motion of each element are given as:

$$\left(-\omega^2 M + i\omega C + K\right)q = f \tag{8}$$

where *M*, *C* and *K* are the mass, damping and stiffness matrices respectively, ω is the natural frequency, *f* is the loading vector and *i* is the imaginary number (Mace et al. 2008).

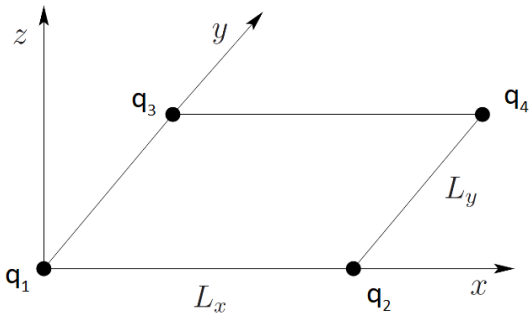

Fig. 2. A rectangular segment with a 4–noded rectangular finite element.

The wave propagation in 2D structures can be considered as a Bloch wave (Bloch 1928), (Floquet 1883). The relation among the periodic displacements q on the sides of the periodic element is given as:

$$q_2 = \lambda_x q_1,\ q_3 = \lambda_y q_1,\ q_4 = \lambda_x \lambda_y q_1, \tag{9}$$

where $\lambda_x = e^{-i\mu_x}$, $\lambda_y = e^{-i\mu_y}$ and the constants $\mu_x = \kappa_x L_x$, $\mu_y = \kappa_y L_y$ $\mu_\chi = \kappa_x L_x$describe the propagation of the wave.

The nodal degrees of freedom can in turn be rewritten as:

$$q = \Lambda_R q_1 \tag{10}$$

where $\Lambda_R = \begin{bmatrix} I & \lambda_x I & \lambda_y I & \lambda_x \lambda_y I \end{bmatrix}$.

In the free response case one has:

$$\Lambda_L f = 0 \tag{11}$$

where $\Lambda_L = \begin{bmatrix} I & \lambda_x^{-1} I & \lambda_y^{-1} I & \lambda_x^{-1} \lambda_y^{-1} I \end{bmatrix}$.

By substituting the equation (10) in the equation (8) and multiplying by $\boldsymbol{\Lambda_L}$, one can take the equation of the free wave motion as:

$$\left(-\omega^2 \bar{M}(\mu_x, \mu_y) + i\omega \bar{C}(\mu_x, \mu_y) + \bar{K}(\mu_x, \mu_y)\right) q = f \tag{12}$$

where $\bar{M} = \Lambda_L M \Lambda_R$, $\bar{C} = \Lambda_L C \Lambda_R$ and $\bar{K} = \Lambda_L K \Lambda_R$ are the reduced mass, damping and stiffness matrices.

The eigenvalue problem is now given as:

$$\bar{D}(\omega, \lambda_x \lambda_y) = 0 \tag{13}$$

where $\bar{D}$ is the reduced dynamic stiffness matrix.

3. Numerical results

In the present investigation a chiral metamaterial which consists of three different materials is considered (see Fig. 3). The first material (grey color) is used for the wings of the unit cell, the second material (green color) is used for the core, while the third softer material (blue color) is used for the rest of the unit cell. The dimensions and material properties of this unit cell are given in Table 1 and 2, respectively.

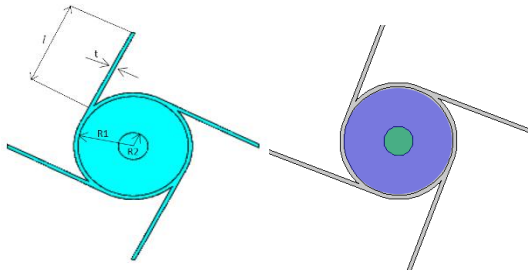

(a) (b)

Fig. 3. (a) Dimensions and (b) material distribution of the chiral unit cell.

Radius R_1	Radius R_2	Length L	thickness t
0.005 m	$R_1/4$ m	0.025 m	0.00035 m

Table 1. Unit cell dimensions

	Material 1	Material 2	Material 3
Young modulus (Pa)	$3.6 \cdot 10^{12}$	$1.1 \cdot 10^{11}$	$5 \cdot 10^{6}$
Density (kg/m^3)	17800	8960	500
Poisson ratio	0.28	0.35	0.48

Table 2. Material properties for the three materials.

3.1 Investigation of chiral metamaterials with and without core

In the first investigation, the dispersion curves for a chiral metamaterial with and without core (see Fig. 4) for the first twenty eigenfrequencies are considered.

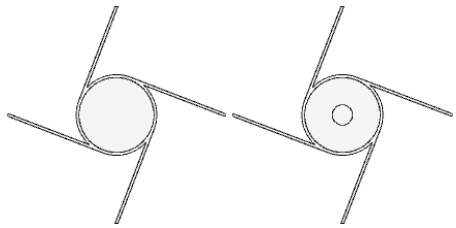

(a) (b)

Fig. 4. Unit cell (a) without core and (b) with core.

As seen in Figs. 5 and 6, several band gaps are created for both models. The largest areas for each case are marked with grey color. In Fig. 5, for the model without core, three band gaps appear between 10kHz and 10.8kHz, between 11.6kHz and 13.8kHz, and between 14.6kHz and

14.8kHz. In Fig. 6, for the model with core, four band gaps appear between 10.1kHz and 10.4kHz, between 10.9kHz and 12.9kHz, between 13.8kHz and 14.6kHz, and between 15.1kHz and 15.4kHz.

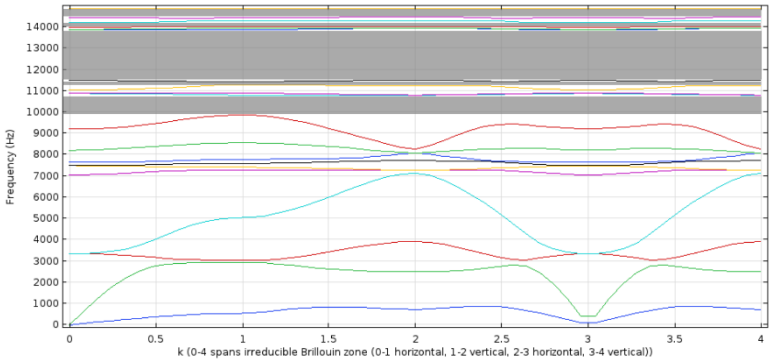

Fig. 5. Dispersion curve for the unit cell without core.

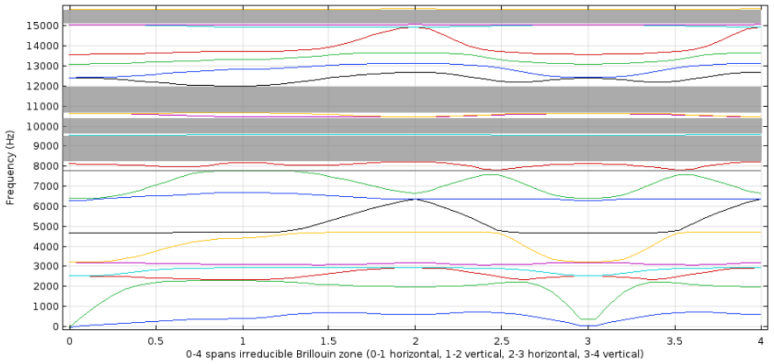

Fig. 6. Dispersion curve for the unit cell with core.

From the results, one can observe that in the case of the unit cell with the core, more band gaps are created, and the range of the first twenty eigenfrequencies is slightly increased. A parametric investigation for the influence of the wing length l to the response of the chiral microstructure with the core will be considered for the microstructure with core.

3.2 Influence of the wing length of chiral metamaterials

Subsequently, the influence of the length l of the chiral wings is investigated. Initially the length of the wing of the chiral unit cell was selected as 0.025 m. Four equidistant cases of ±12.5%, and ±25% of the initial length, that is for lengths equal to 0.01875 m, 0.021875 m, 0.028125 m, and 0.03125 m are considered. The results are presented schematically in Figs. 7, 8, 9 and 10 and numerically in Table 3.

In the first case (l=0.01875 m) the dispersion curve is shown in Fig. 7. One observes that a reduction of 25% on the length of the chiral wing leads to a reduction of the amount of the large band gap areas, however, a significant area appears at lower frequencies.

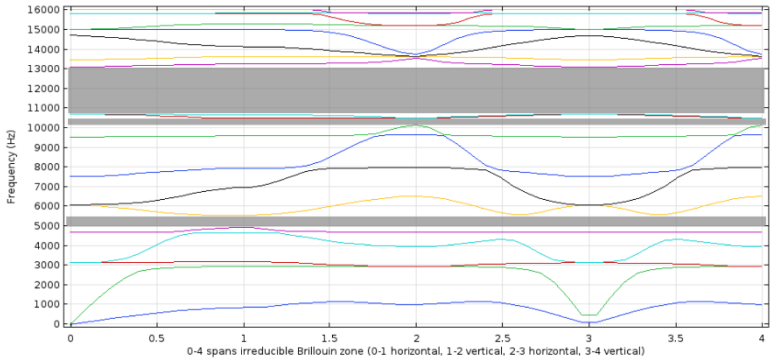

Fig. 7. Dispersion curve for l=0,01875 m.

In the second case (l=0.021875 m) the dispersion curve is shown in Fig. 8. A reduction of 12.5% of the wing length increases the amount of the band gaps, by creating more clear zones, even of smaller size. In this case, the isolation zones appear in high frequencies.

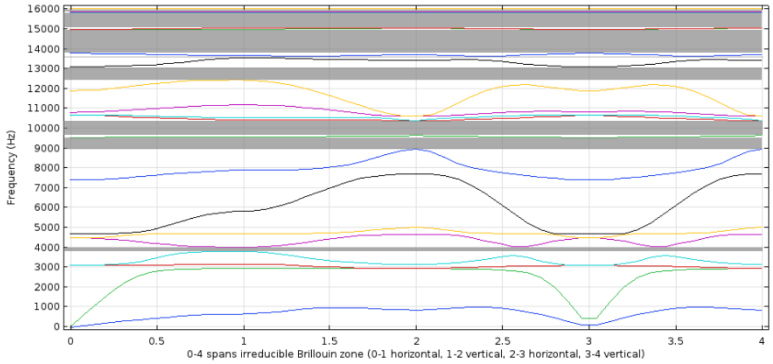

Fig. 8. Dispersion curve for l=0.021875 m.

The dispersion curve for the third case (l=0.028125 m) is shown in Fig. 9. The first significant band gap area appears above 8 kHz, with three discrete zones, very close to each other within the range 8 kHz-12 kHz.

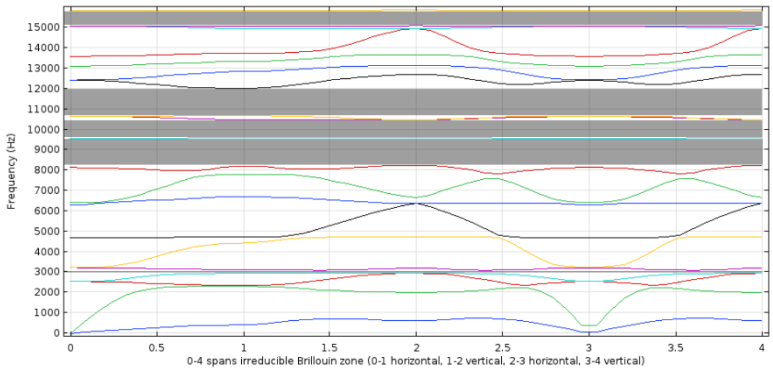

Fig. 9. Dispersion curve for l=0.028125 m.

In the last case the length is increased by 25% (l=0.03125 m). The dispersion curve for this case is shown in Fig. 10 where six large band gaps appear. These zones are equally distributed in two different frequency areas (between 7 kHz – 10 kHz and 12 kHz-15.5 kHz).

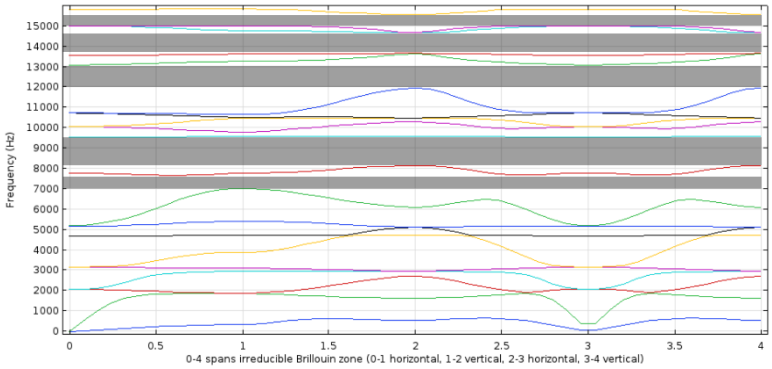

Fig. 10. Dispersion curve for l=0.03125 m.

From the parametric investigation one concludes that the wing length modification affects the band gaps. However, the range of the first twenty eigenfrequencies remains within 0-16 kHz.

	l=0.01875m	l=0.021875m	l=0.025m	l=0.028125m	l=0.03125m
1st bg (Hz)	4675-4701	3805-4018	3030- 3148	2947-3099	7005-7670
2nd bg (Hz)	4930-5550	8950-9550	9505- 9550	7797-7824	8140-9550
3rd bg (Hz)	10150-10490	9634-10382	10025- 10494	8197-9550	9593-9805
4th bg (Hz)	10714-13115	12443-13120	10690- 13111	9615-10488	11956-13096
5th bg (Hz)	-	13553-13635	13346- 13576	10676-12002	13668-14674
6th bg (Hz)	-	13786-14975	13690- 14525	15092-15834	15028-15576
7th bg (Hz)	-	15046-15835	15000- 15390	-	-
8th bg (Hz)	-	15857-16018	-	-	-

Table 3. Numerical results of the parametric investigation for the length of the chiral wing.

3.3 Influence of the radius R_1

In the third instance, the influence of the radius R_1 of the bigger disk (see Fig. 3) is investigated. Initially the radius R_1 was set to 0.005m. Again, four equidistant cases of ±10%, and ±20% of the initial radius were studied. More specifically, radiuses of 0.004m, 0.0045m, 0.0055m, and 0.006m are considered. The results are depicted in Figs. 11, 12, 13 and 14. The numerical results are given in Table 4.

In the first case (R_1=0.004m) the dispersion curve is shown in Fig. 11. One observes that a reduction of 20% of the radius R_1 of the chiral material affects the frequency range of band gaps, as they appear after the frequency of 10kHz. There are six band gap areas, however only four are visible.

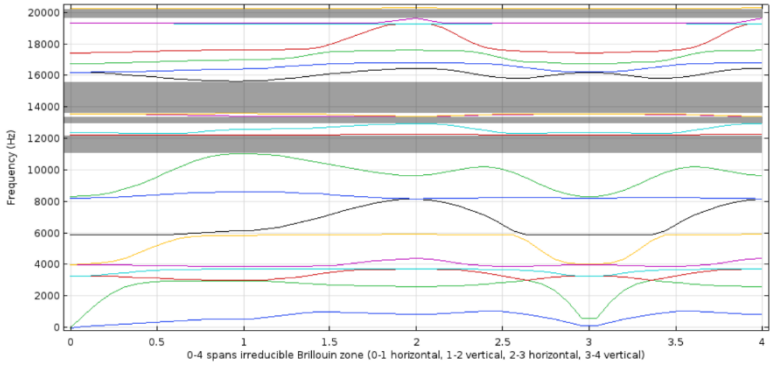

Fig. 11. Dispersion curve for R1=0.004m.

The dispersion curve for the second case (R_1=0.0045m) is shown in Fig. 12. In this case the band gaps are moved in higher frequencies; however, a large band gap area is created within 12kHz and 14.7kHz.

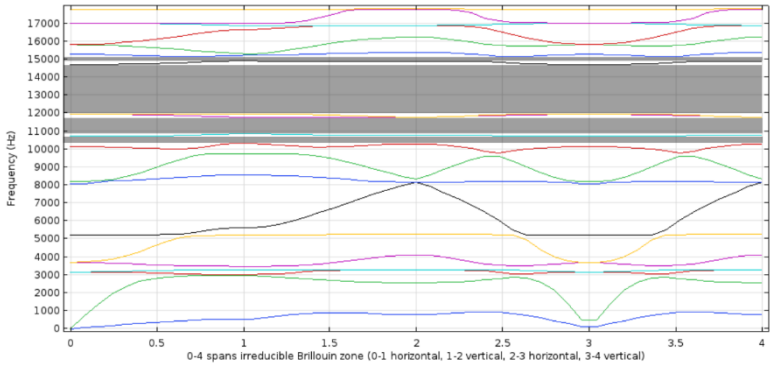

Fig. 12. Dispersion curve for R1=0.0045m.

In the third case of this investigation, that is for radius which is increased by 10% (R_1=0.0055m), we obtain the dispersion curve of Fig. 13. One can observe that the microstructure of this case is very efficient for frequencies between 10kHz and 14kHz. Moreover, a smaller band gap area appears between 7kHz and 8kHz, which is lower than the ones οφ the original case (R_1=0.005m). The number of the zones does not seem to be affected.

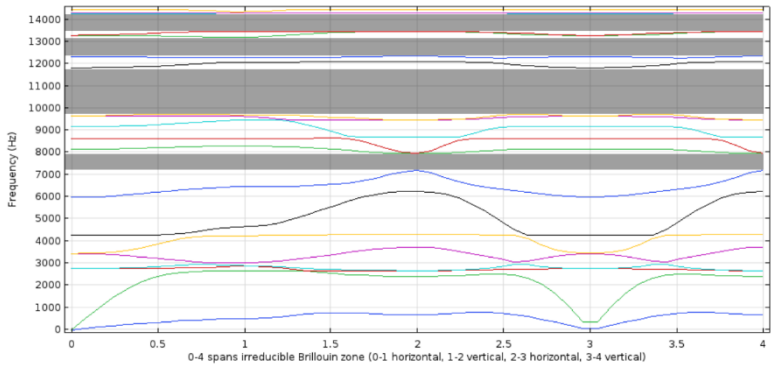

Fig. 13. Dispersion curve for R1=0.0055 m.

In the last case of this subsection, the radius R_1 is increased by 20% (R_1=0.006m). The dispersion curve for this case is shown in Fig. 14 where four large band gap areas appear. These zones are distributed within the frequency range of 2.8kHz - 13kHz. The important thing here is the appearance of two band gaps at lower frequencies, a large between 6.3kHz – 7.8kHz and a smaller between 2.8kHz – 3kHz, which might be useful in some applications. The number of large band gap zones here are increased to five.

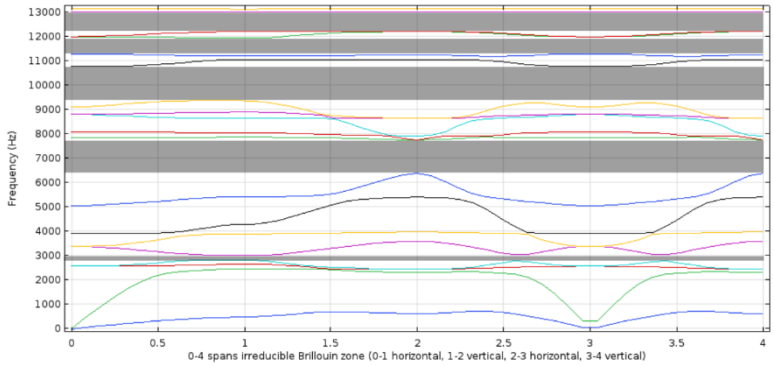

Fig. 14. Dispersion curve for R1=0.006 m.

From the parametric investigation one concludes that the wing length modification affects the band gaps. However, the range of the first twenty eigenfrequencies remains within 0-16kHz.

	R_1=0.004m	R_1=0.0045m	R_1=0.005m	R_1=0.0055m	R_1=0.006m
1st bg (Hz)	3720-3890	2955-3020	3030- 3148	2945-3020	2827-3010
2nd bg (Hz)	11065-12010	3290-3478	9505- 9550	7911-7947	6363-7753
3rd bg (Hz)	12275-12326	9750-9793	10025- 10494	9740-11820	9362-10760
4th bg (Hz)	12955-13425	10320-10722	10690- 13111	12084-12275	11055-11182
5th bg (Hz)	19630-20270	10870-11780	13346- 13576	12345-13200	11285-11926
6th bg (Hz)	-	11972-14717	13690- 14525	13465-14270	12203-12990
7th bg (Hz)	-	14914-15144	15000- 15390	14293-14348	13014-13120
8th bg (Hz)	-	17775-17780	-	-	-

Table 4. Numerical results of the parametric investigation for the radius R_1.

3.4 Influence of the density ρ of the material of the core

In the next investigation, the influence of the density ρ of the material of the core (see Material 2 in Table 2) is studied. Initially the density was set to 8960kg/m^3. Four cases are taken into account, where density is altered at ±10% and ±20% of the initial one. Namely, a density of 7160 kg/m^3, 8060 kg/m^3, 9860 kg/m^3, and 10760 kg/m^3 are considered. The results are shown in Figs. 15, 16, 17 and 18. The numerical results are given in Table 5.

In the first case, the density is decreased by 20% (ρ=7160 kg/m^3) and the dispersion curve is shown in Fig. 15. It is clearly shown that this reduction affects not only the frequency range of band gaps, but also their number, as well as their size. Five visible isolated areas are created, with a large band gap between 10.8k Hz and 13 kHz.

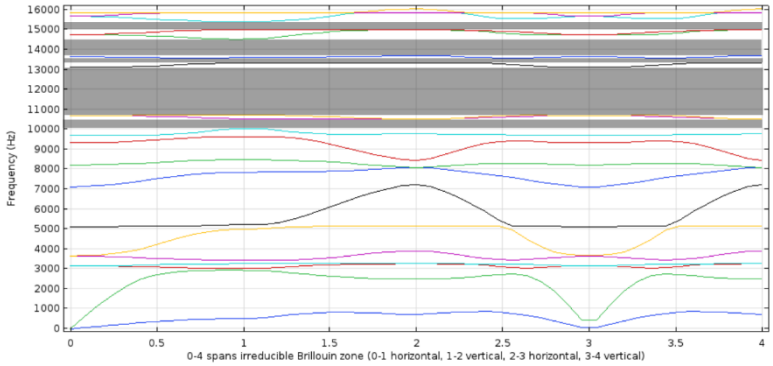

Fig. 15. Dispersion curve for ρ=7160 kg/m^3.

The dispersion curve for the second case (ρ=8060 kg/m^3) is shown in Fig. 16. It is observed that in this case the results are similar with the previous case.

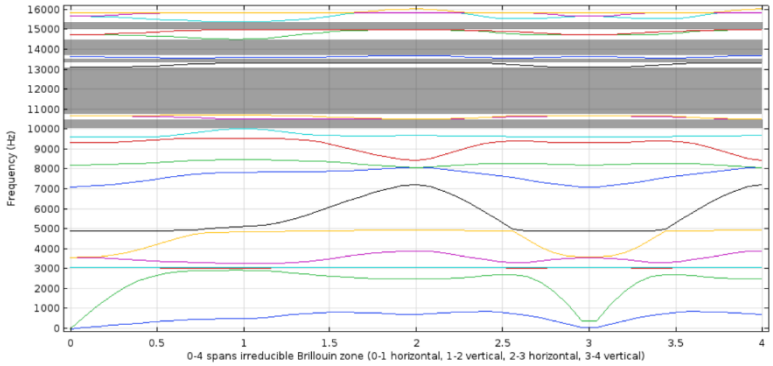

Fig. 16. Dispersion curve for ρ=8060 kg/m^3.

In the third case (ρ=9860k g/m^3), the dispersion curve is depicted in Fig. 17.

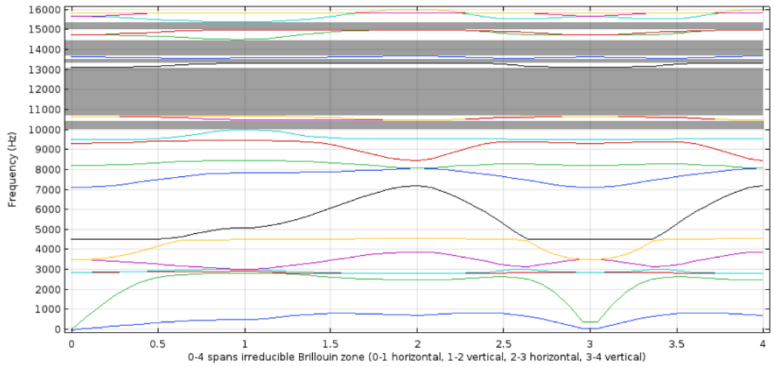

Fig. 17. Dispersion curve for ρ=9860 kg/m^3.

In the last case the density is increased by 20% (ρ=10760 kg/m^3). The dispersion curve for this case is shown in Fig. 18 where again, the results look similar to the ones of the previous cases. This suggests that the number and the range of the band gap zones does not seem to be affected by the modification of the density of the core's material.

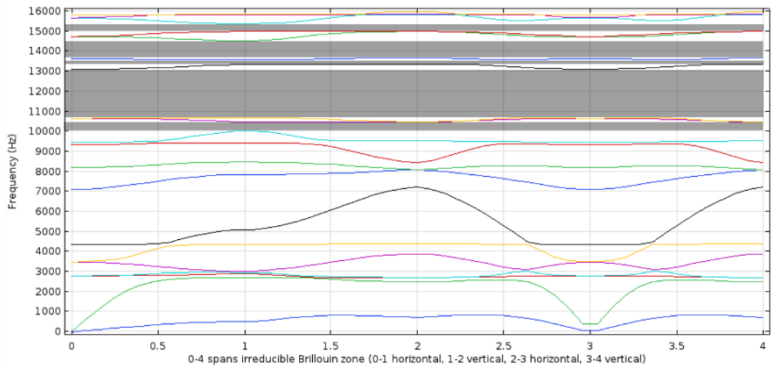

Fig. 18. Dispersion curve for ρ=10760 kg/m^3.

	ρ=7160kg/m^3	ρ=8060kg/m^3	ρ=8960kg/m^3	ρ=9860kg/m^3	ρ=10760kg/m^3
1st bg (Hz)	2935-3028	2933-3030	3030- 3148	9460-9500	3010-3030
2nd bg (Hz)	3260-3443	3091-3285	9505- 9550	10700-13110	9420-9456
3rd bg (Hz)	9630-9700	9562-9617	10025- 10494	13340-13575	10015-10479
4th bg (Hz)	10050-10515	10035-10503	10690- 13111	13690-14525	10693-13110
5th bg (Hz)	10724-13110	10714-13110	13346- 13576	15000-15390	13340-13575
6th bg (Hz)	13340-13575	13340-13575	13690- 14525	-	13690-14525
7th bg (Hz)	13690-14525	13690-14525	15000- 15390	-	15000-15390
8th bg (Hz)	15000-15390	15000-15930	-	-	-

Table 5. Numerical results of the parametric investigation for the density ρ of Material 2.

3.5 Study of a ten-by-ten lattice made of chiral microstructures

In the last investigation, a ten-by-ten lattice, which consists of chiral unit cells is considered, using the material and design properties as mentioned in the Tables 1 and 2 (see Fig. 19).

Two different boundary conditions are applied on the structure. A roller boundary condition, preventing the movement on the vertical axis and leaving free the movement on the horizontal

axis, is applied at the bottom and top sides, while fixed constraints are applied at the right edge of the lattice. At the left edge of the lattice, a harmonic load with amplitude which corresponds to a pressure equals to 10Mpa, is applied with direction on the horizontal axis. The frequency response of the structure under this harmonic load is studied and compared with the dispersion curve.

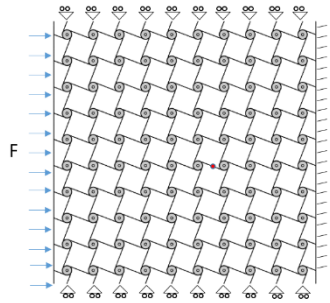

Fig. 19. The 10 by10 lattice, loadings and boundary conditions.

The displacement amplitude of the red point (see Fig. 19) at the band gap areas is equal to zero. One can observe that the approximation of the Bloch theorem is very accurate and effective as it predicted four different zones where oscillation isolation is achieved. These frequency zones appear between 10 kHz-15.3 kHz as seen in Fig. 20.

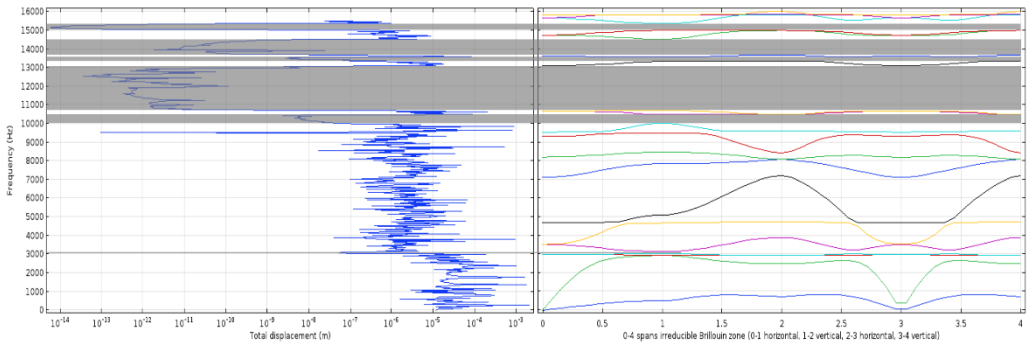

Fig. 20. Frequency response of the lattice and the dispersion curve of the Chiral unit cell.

The band gap areas affect the whole lattice and not only one specific point. For instance, a loading case with a harmonic excitation and frequency outside of the band gap zones (e.g. 14.8kHz) creates strong oscillations in several areas of the lattice and the wave propagates through the medium. On the other hand, the use of a frequency within a band gap zone (e.g. 11kHz) leads to oscillation isolation, which is achieved by preventing the wave propagation before it passes from the second layer of unit cells (see Fig. 21). Thus, the stresses and the displacement of the structure remain in low levels.

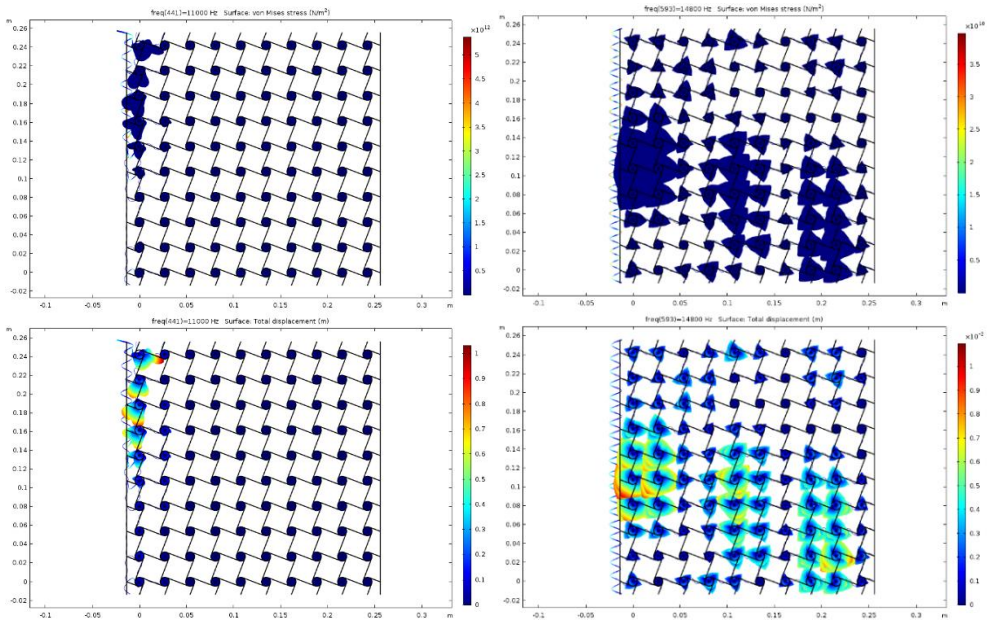

Fig. 21. Stresses and displacements of the lattice inside and outside of the band gap.

4. Conclusions

In the present investigation, a chiral microstructure is studied as a potential vibration isolation medium for certain frequencies. Initially the influence of the use of a different material for the core of the element is investigated, indicating that the metamaterial with the core presents improved behavior in the creation of band gap zones. Subsequently, the length of the chiral wings is modified, in order to study the effect on the band gaps. From the results of the parametric investigation, it was shown that the modification of the geometrical parameters of the chiral material, that is the wing length l and the radius R_1, significantly affects the occurrence of the band gap areas, without intervening on the range of the first twenty eigenfrequencies which remains within 0-16 kHz. On the other hand, the modification of the material properties, and more specifically the alteration of the density of the material of the chiral core, does not seem to affect the appearance of band gaps.

Finally, the application of such metamaterials on a ten-by-ten lattice is considered. The results validate the dispersion curves of the previous investigations. The influence of chirality on band gap properties and, in particular, the transfer of energy between longitudinal and rotational vibration can be studied by using a two-dimensional finite element model. Design for specific demands for a given application and optimal design can be based on this computational procedure. The influence of inclusions and geometry constants, investigated here, as well as of different shapes (Qi et al. 2019) (Xin et al. 2021) and possible piezoelectric enhancements (Koutsianitis et al. 2021), open possibilities for the design of new tailored metamaterials.

Acknowledgement: This research is co-financed by Greece and the European Union (European Social Fund- ESF) through the Operational Programme «Human Resources Development, Education and Lifelong Learning» in the context of the project “Reinforcement of Postdoctoral Researchers - 2nd Cycle” (MIS-5033021), implemented by the State Scholarships Foundation (IKY).

References

Askari M, Hutchins DA, Thomas PJ, Astolfi L, Watson RL, Abdi M, Ricci M, Laureti S, Nie L, Freear S, Wildman R, Tuck C, Clarke M, Woods E, Clare AT (2020). Additive manufacturing of metamaterials: A review, *Additive Manufacturing*, 36, 101562.

Bacigalupo A, De Belis ML (2015). Auxetic anti-tetrachiral materials: Equivalent elastic properties and frequency band-gaps, *Composite Structures*, 131, 530-544.

Bacigalupo A, Lepidi M, Gnecco G, Vadalà F, Gambarotta L (2019). Optimal Design of the Band Structure for Beam Lattice Metamaterials, *Frontiers in Materials*, 6, 2.

Bloch F (1928).Über die Quantenmechanik der Elektronen in Kristallgittern, *Zeitschrift für Physik*, 52, 555-600.

Brillouin L (1953). *Wave Propagation in periodic structures. 2nd ed.*, Dover, New York.

Chen L, Guo Y, Yi H (2021). Optimization study of bandgaps properties for two-dimensional chiral phononic crystals base on lightweight design, *Physics Letters A*, 388, 127054.

Chen W, Tian X, Gao R, Liu S (2018). A low porosity perforated mechanical metamaterial with negative Poisson's ratio and band gaps, *Smart Materials and Structures*, 27, 115010.

Duncan O, Shepherd T, Moroney C, Foster L, Venkatraman PD, Winwood K, Allen T, Alderson A (2018). Review of auxetic materials for sports applications: Expanding options in comfort and protection, *Applied Sciences*, 8, 941.

Fei X, Jin L, Zhang X, Li X, Lu M (2020). Three-dimensional anti-chiral auxetic metamaterial with tunable phononic bandgap, *Applied Physics Letters*, 116, 021902.

Floquet G (1883). Sur les équations différentielles linéaires à coefficients périodiques, *Annales Scientifiques de l'école Normale Supérieure*, 12, 47-88.

Hosseinkhani A, Younesian D, Ranjbar M, Scarpa F (2021). Enhancement of the vibro-acoustic performance of anti-tetra-chiral auxetic sandwich panels using topologically optimized local resonators, *Applied Acoustics*, 177, 107930.

Hsiang-Wen T, Wei-Di C, Lien-Wen C (2017). Wave propagation in the polymer-filled star-shaped honeycomb periodic structure, *Applied Physics A*, 123, 523.

Kittel C (1962). *Elementary solid-state physics: A Short Course. 1st ed.*, Wiley, New York.

Koutsianitis P, Tairidis GK, Drosopoulos GA, Stavroulakis GE (2019). Conventional and star-shaped auxetic materials for the creation of band gaps, *Archive of Applied Mechanics*, 89, 2545-2562.

Koutsianitis PI, Tairidis GK, Stavroulakis GE (2021). Shunted piezoelectric patches on auxetic microstructures for the enhancement of band gaps. *Archive of Applied Mechanics,* 91**,** 739–751 (2021)

Ma Y, Scarpa F, Zhang D, Zhu B, Chen L, Hong J (2013). A nonlinear auxetic structural vibration damper with metal rubber particles, *Smart Materials and Structures*, 22, 084012.

Mace BR, Manconi E (2008). Modelling wave propagation in two-dimensional structures using finite element analysis, *Journal of Sound and Vibrations*, 318, 884-902.

Matlack KH, Bauhofer A, Krödel S, Palermo A, Daraio C (2016). Composite 3D-printed metastructures for low-frequency and broadband vibration absorption, *Proceedings of the National Academy of Sciences of the United States of America*, 113, 8386-8390.

Maurin F, Claeys C, Deckers E, Desmet W (2018). Probability that a band-gap extremum is located on the irreducible Brillouin-zone contour for the 17 different plane crystallographic lattices, *International Journal of Solids and Structures*, 135, 26-36.

Meng J, Deng Z, Zhang K, Xu X, Wen F (2015). Band gap analysis of star-shaped honeycombs with varied Poisson's ratio, *Smart Materials and Structures*, 24, 095011.

Outzen L, Koutsianitis P, Novajan A, Tairidis GK, Langer SC, Stavroulakis GE (2019). Band gap analysis of classical and auxetic composites, 12th HSTAM International Congress on Mechanics, Thessaloniki, Greece, 22-25 September, 2019.

Qi D, Yu H, Hu W, He C, Wu W, Ma Y (2019). Bandgap and wave attenuation mechanisms of innovative reentrant and anti-chiral hybrid auxetic metastructure, *Extreme Mechanics Letters*, 28, 58-68.

Spadoni A, Ruzzene M, Gonella S, Scarpa F (2009). Phononic properties of hexagonal chiral lattices, *Wave Motion*, 46, 435-450.

Srikantha Phani A, Woodhouse J, Fleck NA (2006). Wave propagation in two-dimensional periodic lattices, *The Journal of the Acoustical Society of America*, 119, 1995.

Wu W, Hu W, Qian G, Liao H, Xu X, Berto F (2019). Mechanical design and multifunctional applications of chiral mechanical metamaterials: A review, *Materials & Design*, 180, 107950.

Xin Y, Wang H, Wang C, Cheng S, Zhao Q, Sun Y, Gao H, Ren F (2021) Properties and tunability of band gaps in innovative reentrant and star-shaped hybrid honeycomb metamaterials, *Results in Physics*, 24, 104024.

Yilmaz C (2018). Inertial Amplification Induced Phononic Band Gaps in a Chiral Elastic Metamaterial, 12th International Congress on Artificial Materials for Novel Wave Phenomena (Metamaterials), 451-453.